33. R. E. Twyman, L. C. Gahring, J. Spiess, S. W. Rogers, *Neuron* **14**, 755 (1995).
34. K. Dinkel, H. M. Meinck, K. M. Jury, W. Karges, W. Richter, *Ann. Neurol.* **44**, 194 (1998).
35. H. Baran, W. Loscher, M. Mevissen, *Brain Res.* **652**, 195 (1994).
36. G. K. Steinberg *et al.*, *Neuroscience* **64**, 99 (1995).
37. E. I. Gusev, V. I. Skvortsova, G. A. Izykenova, A. A. Alekseev, S. A. Dambinova, *Zh. Nevropatol. Psikhiatr. Im. S. S. Korsakova* **96**, 68 (1996).
38. N. Aihara, H. Tanno, J. J. Hall, L. H. Pitts, L. J. Noble, *J. Comp. Neurol.* **342**, 481 (1994).
39. W. G. Mayhan and S. P. Didion, *Stroke* **27**, 965 (1996).
40. D. K. Zucker, G. F. Wooten, E. W. Lothman, *Exp. Neurol.* **79**, 422 (1983); S. Albayrak, Q. Zhao, B. K. Siesjo, M. L. Smith, *Acta Neuropathol.* **94**, 158 (1997).
41. M. J. During *et al.*, in preparation.
42. We thank D. Wu, P. Schweder, J. Francis, S. McPhee, and R. Bland for general technical assistance and advice, C. G. Janson, J. Heywood, M. Dragunow, J. Fraser, and K. Lehnert for scientific assistance, helpful discussions, and manuscript review, T. Hughes for the NMDAR1 cDNA, and X. Xiao and R. J. Samulski for the original AAV cloning and packaging plasmids and advice regarding generation of recombinant AAV vectors. Supported in part by the New Zealand Marsden Fund, New Zealand Health Research Council, and the Jefferson Faculty Foundation.

4 November 1999; accepted 21 January 2000

Shaped Ceramics with Tunable Magnetic Properties from Metal-Containing Polymers

Mark J. MacLachlan,[1] Madlen Ginzburg,[1] Neil Coombs,[1] Thomas W. Coyle,[2] Nandyala P. Raju,[3] John E. Greedan,[3] Geoffrey A. Ozin,[1]* Ian Manners[1]*

A shaped, magnetic ceramic was obtained from a metal-containing polymer network, which was synthesized by thermal polymerization of a metal-containing organosilicon monomer. Pyrolysis of a cylinder, shape, or film of the metal-containing polymer precursor produced a low-density magnetic ceramic replica in high yield. The magnetic properties of the shaped ceramic could be tuned between a superparamagnetic and ferromagnetic state by controlling the pyrolysis conditions, with the particular state dependent on the size of iron nanoclusters homogeneously dispersed throughout the carbosilane-graphitic–silicon nitride matrix. These results indicate that cross-linked metal-containing polymers may be useful precursors to ceramic monoliths with tailorable magnetic properties.

High-performance ceramics, such as SiC, AlN, B_4C, and TiN, are of widespread technological importance in applications as diverse as rocket nozzles and automobile parts (*1*–*3*). Ceramics obtained as films, coatings, fibers, or bulk shapes are especially appealing for practical applications. Ceramic materials are generally prepared from powders in a sequence of synthesis, processing, shaping, and sintering steps. Recent studies suggest that organosilicon polymers and inorganic glasses may be more practical precursors to advanced ceramics, as they have the advantage of a three-dimensional network of covalent bonds and ease of processibility familiar to polymer and sol-gel science (*4*–*8*). Most work on polymer-derived ceramics has focused on the mechanical strength and stability of materials, rather than electronic and magnetic properties (*9*–*13*). Furthermore, the ceramic materials previously obtained from metal-containing polymers are powders. Shaped ceramics with tunable magnetic properties may find utility as protective coatings, magnetic recording media, and antistatic shielding.

Although of considerable interest (*7*–*15*), the preparation of nonoxide ceramics from organometallic polymers has been hindered by the synthetic challenge of conveniently preparing well-characterized precursor materials with appreciable molecular weights. The ring-opening polymerization (ROP) of strained [1]silaferrocenophanes (SFP, Fig. 1A) is a well-established route to high–molecular weight poly(ferrocenylsilanes) (PFS, Fig. 1B) (*16*–*18*). Upon pyrolysis at 1000°C under N_2, PFS yields a magnetic ceramic powder but in low yield (30 to 40%) (*19*). The resulting powders contain ferromagnetic iron particles within the SiC-C-Si_3N_4 matrix. We have shown that pyrolysis of nanoscale cylinders of PFS in hexagonal mesoporous silica at 900°C yields iron nanocrystals with a diameter constrained by the width of the channels (*20*).

An important consideration when choosing a ceramic precursor is the ceramic yield because this ultimately determines the utility, bulk properties, and shape retention in the resulting ceramic. Cross-linking preceramic polymers is a prevalent method for increasing the ceramic yields because it reduces the amount of volatile decomposition products. In this regard, we chose to form an example of a cross-linked metal-containing polymer precursor to demonstrate shape retention in the resulting ceramic. This was achieved starting with the spirocyclic [1]silaferrocenophane (SSFP, Fig. 1C) (*21*, *22*).

Differential scanning calorimetry of SSFP displayed a melt at 92°C followed immediately by an exotherm with two peaks, consistent with ROP. When SSFP was heated in a sealed Pyrex polymerization tube under vacuum at 140°C for 12 hours and then at 180°C for 4 hours, it appeared to melt and rapidly became immobile. The resulting orange-red solid was stirred for 48 hours in tetrahydrofuran (THF) under N_2, but only a small amount of material dissolved. Gel permeation chromatography of the soluble fraction showed no polymer; it probably contained only residual monomer and short oligomers.

The cross-linked preceramic polymer network (CPPN) was characterized by powder x-ray diffraction (PXRD), solid-state magic-angle spinning (MAS) nuclear magnetic resonance (NMR) (^{1}H, ^{13}C, and ^{29}Si), thermogravimetric analysis, and pyrolysis mass spectrometry. A PXRD pattern of the CPPN displays two sharp reflections at $2\theta = 12.81°$, $d = 6.90$ Å [full width at half maximum (FWHM) intensity = 0.29° 2θ] and $2\theta = 15.38°$, $d = 5.76$ Å (FWHM = 0.41° 2θ) corresponding to diffraction coherence between iron centers in the cross-linked polymer network. (θ is the angle of incidence of the x-ray beam on the sample, and d is the lattice spacing.) Also observed are some broad halos revealing additional short-range order in the material.

^{1}H MAS NMR of the CPPN showed two peaks centered at 3.9 ppm and 1.8 ppm, attributed to the cyclopentadienyl (Cp) and methylene resonances, respectively. In the ^{13}C cross-polarization MAS (CP-MAS) NMR spectrum of the CPPN (Fig. 2), two resonances associated with the methylene groups of the carbosilane were observed at 18 and 26 ppm. In the Cp region, several peaks observed between 73.2 and 76 ppm are consistent with Cp (C–H) carbons. Also, three

[1]Department of Chemistry, University of Toronto, 80 St. George Street, Toronto, Ontario M5S 3H6, Canada. [2]Department of Metallurgy and Materials Science and Department of Chemical Engineering and Applied Chemistry, University of Toronto, 184 College Street, Toronto, Ontario M5S 3E4, Canada. [3]Brockhouse Institute for Materials Research, McMaster University, Hamilton, Ontario L8S 4M1, Canada.

*To whom correspondence should be addressed. E-mail: gozin@alchemy.chem.utoronto.ca; imanners@alchemy.chem.utoronto.ca

ipso-carbon resonances are observed at 63.8, 66.5, and 67.6 ppm, downfield from the single ipso-carbon resonance observed in the strained monomer SSFP at 31.9 ppm. Assuming that thermal ROP of SSFP proceeds through random ring-opening of both the silacyclobutane and the ferrocenophane rings and that the reactive Cp/CH_2 ends can recombine with any other Si center, there are three Si microenvironments possible in the random cross-linked polymer as shown in Fig. 1D. This is consistent with the observation of three distinct ipso-carbon resonances in the ^{13}C NMR spectrum of the CPPN. Furthermore, the ^{29}Si CP-MAS NMR spectrum displays a sharp peak at 4 ppm and a broader peak at 8 ppm, in accord with this proposal.

When a Pyrex polymerization tube (15-cm length by 1-cm diameter) was loaded with SSFP and heated for 7 hours at 150°C followed by 16 hours at 180°C, a solid sample of the CPPN was obtained that resembled the shape of the glass mold (Fig. 3). The rigid, insoluble rod had a smooth texture and was difficult to cut with a knife. Upon heating to 600°C under N_2, the solid undergoes a small weight loss (90% ceramic yield) and contraction (10%) but retains its overall shape. In addition, the ceramic is hard and is attracted to a bar magnet. The bulk density of a sample was determined to be 1.61 ± 0.01 g cm^{-3}, only slightly more dense than the crystalline precursor SSFP (density = 1.54 g cm^{-3}). Flexible polymer films could also be formed by sublimation of the monomer onto a hot glass tube. Subsequent thermal treatment at 550° to 600°C provides a route to rigid magnetic ceramic films that were also attracted to a bar magnet.

Scanning electron microscopy (SEM) of the bulk ceramic (Fig. 4A) and high-resolution transmission electron microscopy (TEM) reveal a smooth and nonporous texture, which was confirmed by nitrogen adsorption measurements at 77 K. Furthermore, the fact that no change in ceramic yield ($90 \pm 2\%$) has been observed up to 1000°C and the observation that no oxides have been observed in the PXRD of any samples suggest that bulk oxygen incorporation does not occur. As a control, a sample pyrolyzed under air had an observed ceramic yield of 53% and showed only Fe_2O_3 (haematite) and quartz in the PXRD pattern, where the calculated yield based on complete transformation to Fe_2O_3, SiO_2, CO_2, and H_2O is 55%.

PXRD studies of the ceramic product revealed a low-intensity broad peak assigned to the {110} reflection of crystalline α-Fe near $2\theta = 45°$, $d = 2.03$ Å. This is consistent with the observation of Fe_n nanoclusters in the TEM images of the products. TEM images of cross sections of a bulk sample and a film of the bulk ceramic are shown in Fig. 4, B and C, respectively. In the bulk sample, the Fe_n clusters possess an average diameter of 24 ± 16 Å (sample size of 300 particles). Very few clusters over 50 Å in diameter were observed. As clusters smaller than 10 Å could not be resolved, there may still be many extremely small iron clusters not imaged by TEM. In the film sample, which was treated at a lower temperature, the clusters appear to have a lower polydispersity. In both samples, the Fe_n nanoclusters appear to be homogeneously distributed within an amorphous matrix. High-resolution TEM lattice imaging of medium-sized nanoclusters showed that they were crystalline iron.

Magnetic measurements confirmed that the lightweight ceramic contains superparamagnetic iron clusters. The zero-field–cooled magnetic susceptibility versus temperature curve (Fig. 5A) is consistent with the presence of superparamagnetic clusters with a blocking temperature, T_b, of around 30 K. When the superparamagnetic sample is cooled below T_b in the absence of a magnetic field, the magnetic dipoles of the clusters are locked in a random orientation. As the sample is warmed in a magnetic field, the dipoles slowly align. Above T_b, thermally induced fluctuations of the magnetic dipoles dominate, and the clusters behave as superparamagnets.

Mössbauer spectroscopy at 77 K shows two quadrupole doublets (Fig. 5B). The inner quadrupolar doublet with an isomer shift of 0.27 ± 0.03 mm s^{-1} and a quadrupolar splitting of 2.24 ± 0.03 mm s^{-1} is consistent with the presence of superparamagnetic iron clusters. This doublet results when the rapidly fluctuating magnetic dipoles average the internal hyperfine field of the iron nanoclusters. The room-temperature spectrum is virtually identical to the spectrum at 77 K with only small changes in the isomer shift and quadrupolar splitting of the two doublets. Because of its similarity to the Mössbauer spectrum of ferrocene [isomer shift = 0.46 ± 0.01 mm s^{-1}, quadrupolar splitting = 2.40 ± 0.01 mm s^{-1} (*23*)], the outer doublet (isomer shift = 0.44 ± 0.03 mm s^{-1}, quadrupolar splitting = 2.24 ± 0.03 mm s^{-1}) may be assigned to either iron atoms on the surface of the clusters or atomic iron in a ferrocene-like environment. Reflectance ultraviolet-visible/near-infrared (IR) spectroscopy revealed no d-d absorption as observed in the polymer precursor (440 to 500 nm) and the absence of the C–H stretching overtone at 1665 nm (6006 cm^{-1}) (both observed in samples treated at 550°C or less, but not in any samples treated above 550°C). Furthermore, the IR spectrum of the sample shows virtually no C–H stretching modes for cyclopentadienyl ligands (3100 cm^{-1}), a marked reduction in the C–H stretching region of the alkyl groups (2800 to 3000 cm^{-1}), and a drastic change between 400 and 1500 cm^{-1} (C–C and C=C stretching; ferrocene modes). From this combination of results, we conclude that the ferrocene units have broken up to release all of the iron as clusters.

Hence, the two sets of quadrupolar doublets in the Mössbauer spectrum are best associated with the surface and bulk iron atoms in the superparamagnetic clusters. The higher electric field gradient of the surface compared with bulk iron atoms in the clusters gives rise to the doublet with the larger qua-

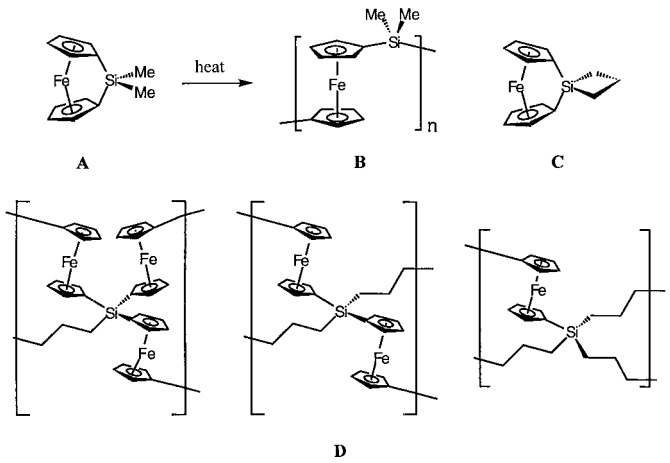

Fig. 1. Structural diagrams. Ring-opening polymerization of SFP (**A**) yields polymer PFS (**B**). When spirocyclic SSFP (**C**) is polymerized, it generates a cross-linked network, CPPN. (**D**) The three possible Si microenvironments for the CPPN.

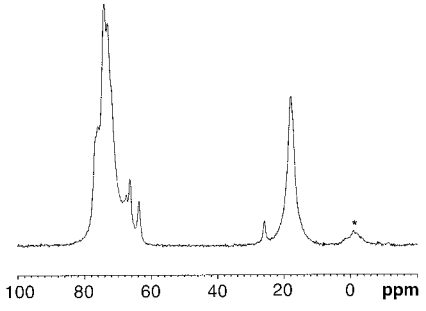

Fig. 2. NMR spectrum. $^{13}C(^1H)$ CP-MAS solid-state NMR spectrum (100.62 MHz; 7.5-kHz spinning rate; 1-ms contact time; and 2-s recycle delay) of the CPPN (spinning side bands are indicated by an asterisk).

drupolar splitting. The much higher intensity doublet of the surface iron in the cluster is consistent with the PXRD, TEM, and magnetization data that show that the clusters are very small. From integration of the area of the doublets, the ratio of surface iron atoms to bulk iron atoms (assuming identical recoil-free fractions) is 2.9. Assuming a spherical body-centered cubic packing model (α-Fe) for the clusters, we calculate that the mean cluster diameter is about 25 Å.

We studied the genesis and microstructure of the ceramic over the temperature range 25° to 1000°C using diffraction, microscopy, spectroscopy, and thermal methods of analysis (*24*). Under a nitrogen atmosphere, the ceramic yield is greater than 90%, and the only volatile components that we were able to detect (NMR and mass spectrometry) are a trace of ferrocene and a molecular species with a mass-to-charge ratio < 500. Starting with the poly(ferrocenylsilane) CPPN, one observes with increasing pyrolysis temperature the formation (600°C) of superparamagnetic iron clusters dispersed within an amorphous "carbosilane" matrix, which gradually transforms (700°C) into larger clusters embedded in a composite "carbosilane-graphite" matrix. Above 900°C, small amounts of SiC and Si_3N_4 are formed. Vibrational spectroscopy indicates that within the detection limit of the technique, samples treated above 600°C are devoid of covalently bound hydrogen.

As the pyrolysis temperature was increased, we observed an increased Fe_n particle size by PXRD and TEM (*24*). Magnetization versus field data were collected for the lightweight ceramics prepared at 650°, 850°, and 1000°C. Magnetization measurements of ceramics formed at 650° and 850°C (Fig. 5C) show virtually no hysteresis at 100 or 300 K, characteristic of superparamagnetic clusters. Moreover, the approach to magnetic saturation was slow for these ceramics. However, the ceramic

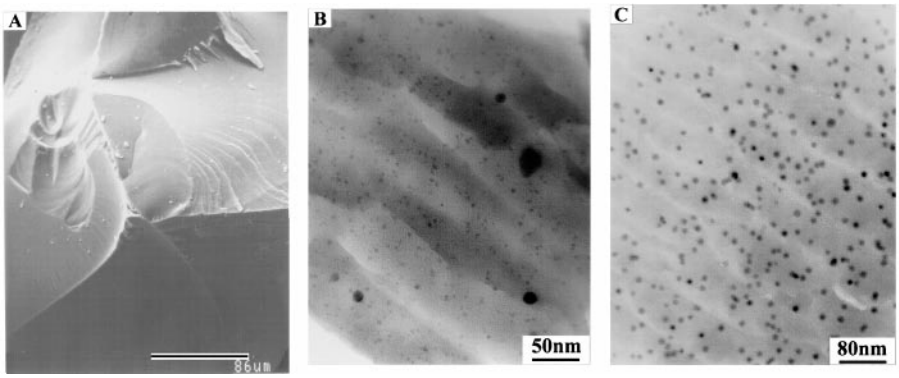

Fig. 4. Electron microscopy. (**A**) SEM image of the bulk ceramic obtained from the pyrolysis of CPPN at 600°C. (**B** and **C**) TEM images of a cross section of (B) the ceramic shape obtained from pyrolysis of the CPPN at 600°C and (C) a film of the ceramic obtained from pyrolysis of the CPPN at 550°C.

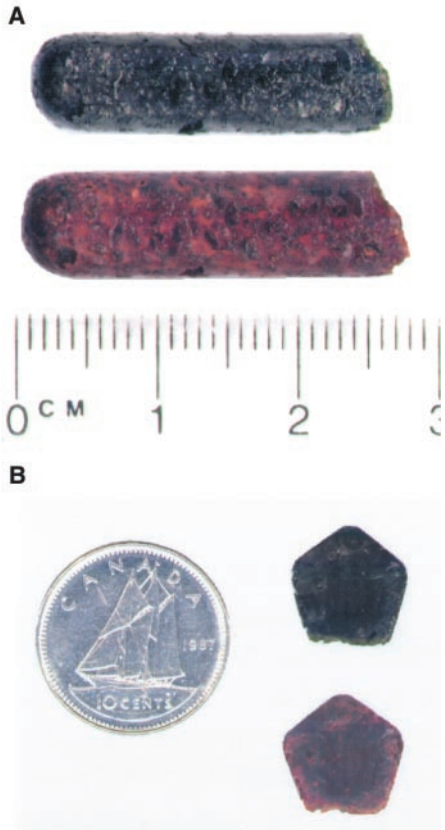

Fig. 3. (**A**) Photographs of the bulk organometallic polymer before (bottom) and after (top) pyrolysis at 600°C. (**B**) Photographs of the CPPN cast in a pentagonal Teflon mold before (bottom) and after (top) pyrolysis at 600°C. The ceramics retain the shape of the precursor polymer and show only a small contraction after pyrolysis (pyrolysis was not performed in a mold).

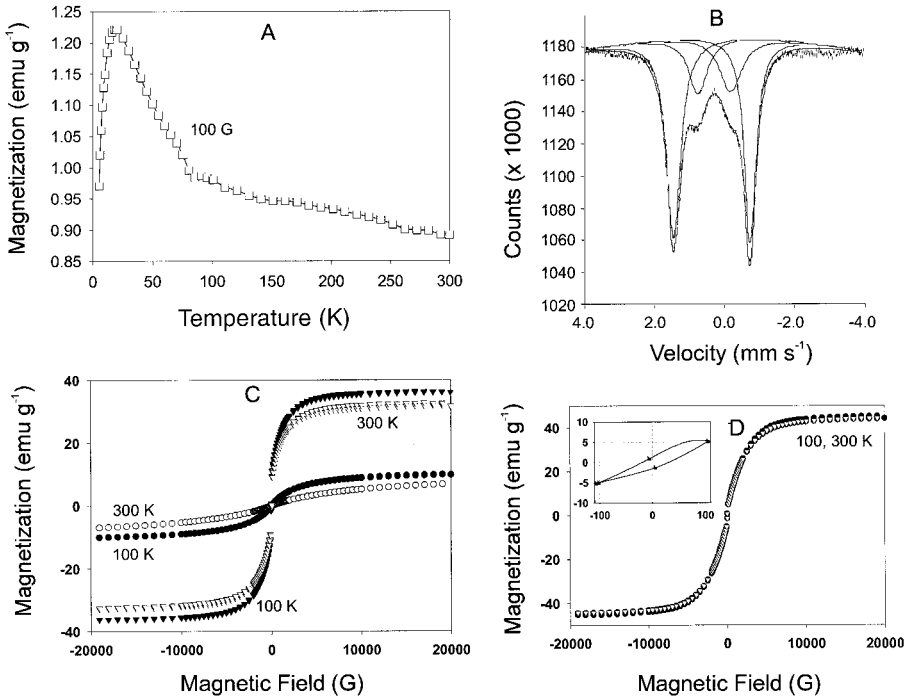

Fig. 5. (**A**) Zero-field–cooled magnetization versus temperature at constant field (100 G) for a sample of the bulk ceramic obtained at 600°C. The magnetic dipoles of the Fe_n nanoclusters are spatially locked below T_b. An applied magnetic field allows the magnetic dipoles of the clusters to align as the sample is warmed to T_b. Above T_b, the rapid fluctuation of magnetic dipoles gives rise to superparamagnetic behavior. The material then obeys the Curie law with Boltzmann thermal randomization of the fluctuating magnetic dipoles. (**B**) The Mössbauer spectrum of the sample at 77 K fit with two quadrupolar doublets. (**C**) Magnetization versus field measurements for ceramic samples prepared at 650°C [at 100 K (●) and 300 K (○)] and 850°C [at 100 K (▼) and 300 K (▽)]. (**D**) Magnetization versus field measurements for a ceramic sample prepared at 1000°C [at 100 K (●) and 300 K (▽)]. The inset is an expanded region of (D) that shows that the ceramic displays room-temperature hysteresis with a small remanent magnetization. emu, electromagnetic unit.

prepared at 1000°C rapidly reached saturation and displayed room-temperature hysteresis (with a small remanence) in its magnetization, as shown in Fig. 5D. This is characteristic of a ceramic material in which the Fe_n clusters have become just large enough to display ferromagnetism. Thus, in ceramics prepared below 900°C, the iron nanoclusters are superparamagnetic, whereas ceramics prepared at higher temperatures contain larger iron clusters that are ferromagnetic. By varying the pyrolysis temperature and time of the polymer precursor, we can control the magnetic properties of the resulting ceramic.

Nanoindentation measurements provided values of the Young's modulus E for the superparamagnetic ceramic formed at 850°C (29.4 GPa) and the ferromagnetic ceramic formed at 1000°C (15.4 GPa). For comparison, the Young's modulus for the polymer precursor CPPN was $E = 6.9$ GPa. The values for the magnetic ceramics are greater than that of graphite ($E = 4.8$ GPa) and are in the same region as that of borosilicate glass ($E = 17.5$ GPa) (*25*).

This report illustrates a metal-containing organosilicon polymer network that functions as a controlled iron delivery vehicle and as a matrix for the nucleation and growth of iron nanoclusters. The ceramics can be molded into shapes and may exhibit interesting magnetic, electrical, and optical properties.

References and Notes

1. H.-P. Baldus and M. Jansen, *Angew. Chem. Int. Ed. Engl.* **36**, 328 (1997).
2. J. Bill and F. Aldinger, *Adv. Mater.* **7**, 775 (1995).
3. D. Segal, *Chemical Synthesis of Advanced Ceramic Materials* (Cambridge Univ. Press, New York, 1991).
4. M. Peuckert, T. Vaahs, M. Brück, *Adv. Mater.* **2**, 398 (1990).
5. R. M. Laine and F. Babonneau, *Chem. Mater.* **5**, 260 (1993).
6. T. Wideman, E. E. Remsen, E. Cortez, V. L. Chlanda, L. G. Sneddon, *Chem. Mater.* **10**, 412 (1998).
7. G. T. Visscher, D. C. Nesting, J. V. Badding, P. A. Bianconi, *Science* **260**, 1496 (1993).
8. J. He, M. Scarlete, J. F. Harrod, *J. Am. Ceram. Soc.* **78**, 3009 (1995).
9. S. Bourg, B. Boury, R. J. P. Corriu, *J. Mater. Chem.* **8**, 1001 (1998).
10. E. J. Houser and T. M. Keller, *Macromolecules* **31**, 4038 (1998).
11. Q. Liu, W. Shi, F. Babonneau, L. V. Interrante, *Chem. Mater.* **9**, 2434 (1997).
12. S. Yajima and M. Omori, *Nature* **267**, 823 (1977).
13. D. Thompson, *Nature* **389**, 675 (1997).
14. R. Riedel *et al.*, *Nature* **382**, 796 (1996).
15. I. Manners, *Angew. Chem. Int. Ed. Engl.* **35**, 1602 (1996).
16. D. A. Foucher, B.-Z. Tang, I. Manners, *J. Am. Chem. Soc.* **114**, 6246 (1992).
17. I. Manners, *Chem. Commun.* **1999**, 857 (1999).
18. _____, *Can. J. Chem.* **76**, 371 (1998).
19. R. Petersen *et al.*, *Chem. Mater.* **7**, 2045 (1995).
20. M. J. MacLachlan, P. Aroca, N. Coombs, I. Manners, G. A. Ozin, *Adv. Mater.* **10**, 144 (1998).
21. M. J. MacLachlan, A. J. Lough, W. E. Geiger, I. Manners, *Organometallics* **17**, 1873 (1998).
22. The ceramics exhibiting shape retention were obtained as follows. A Pyrex glass tube was loaded with 2.2 g (8.7 mmol) of SSFP and sealed under vacuum. The sample was heated for 7 hours at 150°C, followed by 16 hours at 180°C. After cooling to room temperature, the tube was broken open to give a rigid, cylindrical sample of CPPN that replicated the shape of the Pyrex polymerization tube. The sample was stirred in THF for 24 hours, but virtually no material dissolved. Next, a section of the orange-red shaped ceramic precursor (1.506 g) was dried under vacuum and then placed in a quartz boat inside a tube furnace. The sample was heated to 600°C over 4 hours and maintained at that temperature for 1 hour under a gentle flow of nitrogen (about 10 ml min^{-1}). A black, lustrous ceramic that appeared identical in shape to the precursor was obtained (1.351 g, 90% yield). Ceramics were also prepared at higher temperatures (every 50°C up to 1000°C) under similar conditions. Yields of 90 ± 2% were obtained in each case.
23. L. M. Epstein, *J. Chem. Phys.* **36**, 2731 (1962).
24. We have studied the genesis of the ceramic in great detail using a multianalytical diffraction, microscopy, spectroscopy and thermal analysis approach, over the temperature range 25° to 1000°C. Full details of this study will be published later. For reference purposes, key data are included in supplementary material (available at www.sciencemag.org/feature/data/1047398.shl).
25. J. F. Shackelford, W. Alexander, J. S. Park, Eds., *CRC Materials Science and Engineering Handbook* (CRC Press, Boca Raton, FL, ed. 2, 1994), p.514.

26. We acknowledge C. Berry for gas adsorption measurements and G. Favoro for nanoindentation measurements. We thank the Natural Sciences and Engineering Research Council (NSERC) of Canada for financial support. The Mössbauer data provided by C. Jones are appreciated. M.J.M. thanks NSERC for a postgraduate scholarship (1995–99). I.M. thanks the Ontario Government for a PREA Award (1999–2004), NSERC for an E. W. R. Steacie Fellowship (1997–99), and the University of Toronto for a McLean Fellowship (1997–2003). G.A.O. thanks the Killam Foundation for an Isaac Walton Killam Foundation Fellowship (1995–97).

26 November 1999; accepted 5 January 2000

Superplastic Extensibility of Nanocrystalline Copper at Room Temperature

L. Lu,[1] M. L. Sui,[2] K. Lu[1]*

A bulk nanocrystalline (nc) pure copper with high purity and high density was synthesized by electrodeposition. An extreme extensibility (elongation exceeds 5000%) without a strain hardening effect was observed when the nc copper specimen was rolled at room temperature. Microstructure analysis suggests that the superplastic extensibility of the nc copper originates from a deformation mechanism dominated by grain boundary activities rather than lattice dislocation, which is also supported by tensile creep studies at room temperature. This behavior demonstrates new possibilities for scientific and technological advancements with nc materials.

Plastic deformation in polycrystalline solids occurs by movement of lattice dislocations and/or diffusional creep. The dislocation movement mechanism predominates in most conventional materials at relatively low temperatures when atomic diffusivity is minor. A strain-hardening effect is always associated with this mechanism, which arises from the pileup of lattice dislocations blocked at grain boundaries. The strain-hardening effect often restricts the mechanical processing of metals, which must be eliminated by thermal annealing in order to perform further deformation without crack formation. Plastic deformation occurs at higher temperatures when atomic diffusivity is considerably increased (at grain boundaries or inside the lattice); in this case, diffusion creep becomes a dominant mechanism. The diffusion creep rate ($\dot{\varepsilon}$), which is dominated by grain boundary diffusion, is related to grain size by (*1*)

$$\dot{\varepsilon} = \frac{B\Omega\sigma\delta D_{gb}}{d^3 kT}$$

where σ is tensile stress, Ω is atomic volume, d is average grain size, B is a numerical constant, D_{gb} is grain boundary diffusivity, δ is grain boundary thickness, and k is Boltzmann's constant. This relation suggests that diffusional creep may be enhanced when grain size is reduced and/or grain boundary diffusivity is enhanced. Based on this mechanism, a decade ago Gleiter *et al.* (*2, 3*) predicted that a nanocrystalline (nc) material, one in which the crystallite size is in the nanometer regime, would make it amenable to high creep rates and large-scale deformation at much lower homologous temperatures, so that ductile ceramics and diffusional creep of pure metals would be possible even at room temperature (*3*). This possibility is of great interest because not only may it shed light on the deformation mechanism of the nanostructure, but it also may significantly facilitate the fabrication process for producing components with complex shapes. Such

[1]State Key Laboratory for Rapidly Solidified Nonequilibrium Alloys, [2]Laboratory for Atomic Imaging of Solids, Institute of Metal Research, Chinese Academy of Sciences, Shenyang 110015, People's Republic of China.

*To whom correspondence should be addressed. E-mail: kelu@imr.ac.cn